SEGMENTED FOIL SEM GRIDS FOR HIGH-INTENSITY PROTON BEAMS AT FERMILAB*

Sacha Kopp#, Bruce Baller, Sam Childress, Richard Ford, Deborah Harris, Dharma Indurthy, Cary Kendziora, Craig Moore, Žarko Pavlović, Marek Proga, Gianni Tassotto, Robert Zwaska.

Abstract

We present recent beam data from a new design of a profile monitor for proton beams at Fermilab. The monitors, consisting of grids of segmented Ti foils 5μm thick, are secondary-electron emission monitors (SEM's). We review data on the device's precision on beam centroid position, beam width, and on beam loss associated with the SEM material placed in the beam.

INTRODUCTION

The extracted beam transport lines and transfer lines between accelerators at Fermilab must operate at ever higher proton fluences to service the neutrino program and the production of antiprotons for the Tevatron collider program. Fig. 1 shows schematically a portion of the Fermilab accelerator complex. The 400 MeV linac supplies beam to the 8 GeV Booster accelerator and is also foreseen to service an extracted beam line to study muon ionization cooling. The Booster delivers beam to the Booster Neutrino Beam (BNB) servicing the MiniBooNE experiment [1]. The Booster is also used to fill the Main Injector with 7 and hopefully up to 11 batches of protons for acceleration to 120 GeV. These 120 GeV protons are split between antiproton production and "Neutrinos at the Main Injector (NuMI)" facility [2].

Design intensity for NuMI beamline is 4×10^{13} protons per spill, with repetition rate of 0.53Hz and transverse beam size of ~1mm.

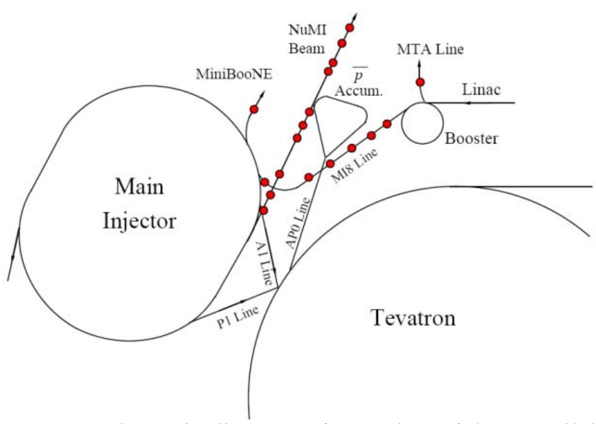

Figure 1: Schematic diagram of a portion of the Fermilab accelerator complex including the 400 MeV linac, 8 GeV Booster, 120 GeV Main Injector, and the extracted beam lines for the Neutrinos at the Main Injector (NuMI), MiniBooNE experiment, and the Muon-Cooling Test Area (MTA). Stations already or soon to be instrumented with foil SEM's are indicated by the circles.

Such fluences place stringent criteria on invasive instrumentation to measure proton beam profiles. Currently at Fermilab, they are measured with Secondary-electron Emission Monitors (SEM's) made from grids of 75μm Ø Tungsten wires [3], which at 1 mm pitch place sufficient amount of material to cause significant fractional loss of beam particles into nearby magnets. The desirability of being able to perform diagnostic measurements while the beams are operated at their nominal intensities motivated lower-mass SEM design.

Based on a design from CERN [4] we have built SEM's consisting of Ti foils. The foil SEM's provide several features over the 75μm Ø Au-plated W-wire SEM's currently in use at FNAL: (1) a factor 50-60 lower fractional beam loss, which is important for reduced component activation or groundwater contamination; (2) greater longevity of Ti signal yield [5], as compared with W or Au-W, which degraded by 20% over the course of running the KTeV fixed-target experiment [3]; (3) a 'bayonnette'-style frame permitting insertion/retraction from the beam without interruption of operations; and (4) reduced calculated beam-heating from the high-intensity proton-pulses, which results in less sag [6].

SEM CHAMBER DESIGN

A view of the foil SEM paddle is shown in Figs. 2 and 3. Three planes of solid Ti foil, 2.5μm in thickness, are interleaved with segmented foils intended for X and Y profiles. The signal foils are 5μm thick. Over the 8cm diameter area of the SEM traversed by the beam, the signal foil strips are 0.15 mm in width. A total of 44 strips are etched into the foil, along with 1.5cm wide strips to measure beam halo out to 3.8cm radius.

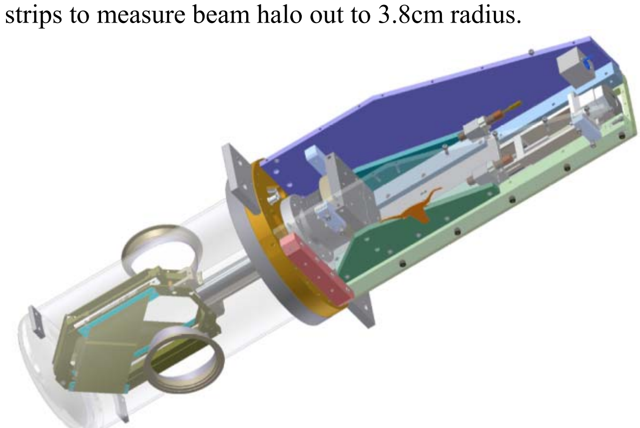

Figure. 2. Drawing of the SEM vacuum chamber. The evacuated portion of the chamber is shown with semi-transparent walls to illustrate the location of the internal foil paddle.

*Work supported by U.S.DoE, contracts DE-FG03-93ER40757 and DE-AC02-76CH3000
#kopp@hep.utexas.edu

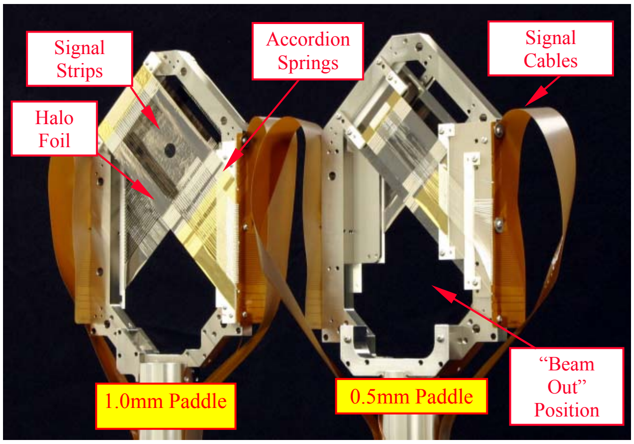

Figure.3: Photograph of a 1.0 mm pitch and a 0.5 mm pitch foil paddle. The paddles have two planes of strips for X and Y profile measurements.

The paddle completely surrounds the beam, so the foils may be inserted into the beam or retracted without the paddle frame traversing the beam. The foils are mounted on precise ceramic combs which define the strip pitch and the foil location on the paddle [7]. A "beam hole" of 12 mm diameter in the bias foil permits most of the 1 mm beam spot to pass through without beam loss, while still permitting adequate voltage bias to maintain signal yield.

Each signal strip has accordion springs pressed into its ends. The springs are elongated by approximately 4 mm prior to installation on the paddle. At this extension, our measurements indicate a tension of ~1g is attained on each strip. The mechanical sag was estimated to be δy=40μm.

The foil actuating mechanism and vacuum can are shown in Fig. 2. The foil paddle is cantilevered on a 5cm diameter hollow shaft, the other end of which is welded to a 12cm "conflat" flange. A linear motion stage and stepper motor actuate the assembly into or out of the beam. A 9cm outer diameter, 6.4cm inner diameter bellows forms the vacuum seal for the actuator. Ceramic-insulated limit switches halt the stepper travel at either end, while a linear variable differential transformer (LVDT) confirms the final beam "in" position of the foils with 1μm accuracy. Kapton-insulated signal cables are routed through the hollow shaft to feedthroughs at its end. The cables are bonded to the foil strips using a conducting epoxy appropriate for ultra-high vacuum, which is also how the strips are bonded to the ceramics. Brackets mount the linear stage to the large 25cm diameter conflat flange on the end of the SEM's vacuum chamber. Precise dowel holes in the 25cm flange and in the moving flange at the end of the bellows allow in situ optical survey of the foil position when installed in the beam line. The 16 liter vacuum chamber is 20cm diameter cylinder with 10cm diameter quick-disconnect flanges at the beam ports.

Each foil plane is measured after mounting on its paddle for mechanical accuracy. Measurements of strip-to-strip pitch are made by analysis of digital photographs suggesting better than 20μm pitch accuracy.

THERMAL SIMULATIONS

We have performed detailed finite element calculations of the temperature induced in the foil SEM's due to heating by the NuMI beam [6]. The heat input to the SEM comes from the energy lost by the beam, and the power dissipated by the SEM comes from blackbody radiation and from thermal conduction through the SEM material. We performed the calculations for several materials. We also compared the heating of wires and foils; wire SEM's cool less efficiently because blackbody radiation is proportional to the surface area of the emitter.

The temperature rise in the SEM material results from ionization energy loss by the 120GeV protons. We used "restricted energy loss" [9] to account for the fact that some δ rays escape out the back of the SEM, so do not deposit their energy in the SEM. The effect of restricted energy loss is greater for thin foils than for wire SEM's and tends to lower the predicted energy deposited in the foil SEM. Fig. 4 shows the results of the thermal model for a 5 μm thick Ti foil. The left plot shows the temperature profile along the center-most strip at several times during the 1.9sec beam cycle, after many transpired beam cycles. As seen in the graph, the beam causes a sharp rise in temperature at *t*=0 sec. The cooling between spills is predominantly due to blackbody radiation. The (small) effect of thermal conduction is evident by the broadening temperature profile over the course of the cooling cycle. The right graph shows the linear expansion of the foil strip, and compares to the elongation expected for a Ti wire 50 μm in diameter.

We compared various materials and looked at the temperature rise Δ*T*, maximum linear elongation Δ*L*, as well as dynamic stress. The dynamic stress may be compared to the "yield stress" for the material, the point at which the material may deform plastically. Beryllium, Carbon fiber and Titanium are preferable from the point of view of long term material damage, *ie*: have dynamic stress values below the yield stress.

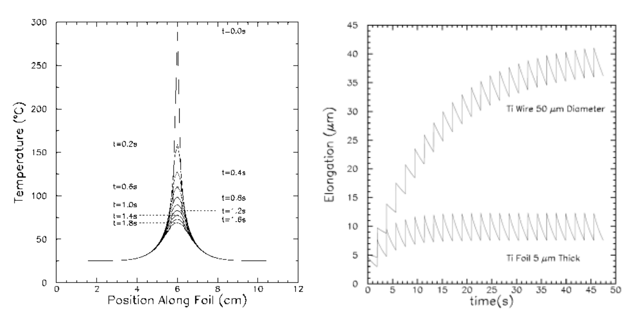

Figure 4: Results of the thermal model of 5μm Ti foil in the NuMI beam. (left) Temperature along the center most strip at several time increments through one beam cycle: at t=0sec the beam passes through the foil, and at then it cools down till next spill arrives 1.9sec later. (right) Net elongation of a 12cm long, 5μm thick, Ti foil strip as a function of time, showing the repeated heating and cooling of several beam cycles. The Ti foil's elongation is compared to that for a 50 μm diameter Ti wire.

The Ti foil SEM experiences 12μm elongation. Because of the 4 mm extension in the accordion springs, we note that this elongation results in <1% tension loss. Of note as well is the fact that a W-wire SEM, when strung on a frame at the maximum stress (the yield stress), stretches the wires by 160μm; thus, beam heating will drop the tension of such a wire SEM by nearly ⅓. Such loss motivates the accordion springs for the foil SEM or individual springs on wire SEM's as has been used by previous workers [11].

IN-BEAM PERFORMANCE

The resolution of the foil SEM grids has been studied previously using a prototype chamber installed in the 8 GeV transfer line to the MiniBooNE experiment [8]. The MiniBooNE beam has transverse size varying from 3mm to 8mm and intensity $(4\text{-}5)\times10^{12}$ppp. The observed resolution on beam centroid and width measurements was compared to a model of the chamber's response which included electronics noise and uncertainties in the foil strips' placement.

More recently, data from the 120 GeV NuMI line has been available. The NuMI beam has ~1mm beam size, affording comparison to the model at a different transverse beam size and also different beam intensity from the data in [8]. Fig. 5 shows data from two adjacent foil SEM's in the NuMI line. The SEM's are approximately 14 m apart with no intervening magnets. The left plot, showing data over the period of a few weeks, shows some variation in the correlation between the two chambers, probably reflecting different beam angles. The right plot shows a 1-dimensional histogram of that data. Interpreting the scatter as arising purely from device resolution, we see that the SEM resolution on centroid is approximately $38\mu m/\sqrt{2}=27\mu m$, consistent with the expectations of [8]. Comparing the beam width as measured by the two monitors suggests the beam width resolution of 20μm.

The primary motivation for the foil SEM's was the possibility to perform invasive beam measurements with reduced fraction beam loss as compared to the previous available instrumentation at FNAL. We compared the beam loss as measured by two ionization chamber loss monitors downstream of a pair of SEM chambers. The two chambers, PM117 and PM118, were both removed and then sequentially re-inserted into the beam. PM118 is a Tungsten-wire SEM (25μmØ), while PM117 is a Ti foil SEM (both are 1.0mm pitch). The relative increase in observed loss at both stations indicates that that PM118 causes approximately 5.9 times more loss than PM117. These measurements indicate that the foil SEM's reduce the beam loss relative to the 75μmØ W wire SEM's [4] by a factor ~50-60. Such reduction will permit profile measurements to be peformed at full design intensity for the transfer lines. Such has proven to be important, as many diagnostics have heretofore been possible only at low intensity.

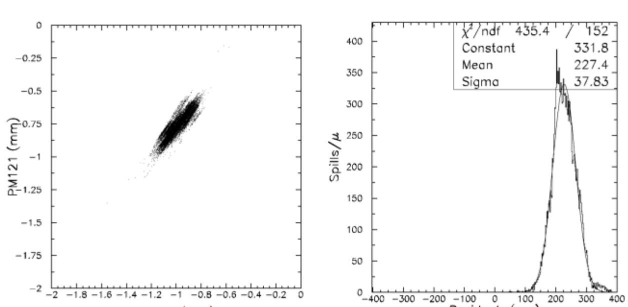

Figure 5: (left) Scatter plot of beam positions as detected by two adjacent foil SEM's in the NuMI beam line. Each point represents one beam spill at 5×10^{12} protons/pulse. The scatter arises in part from beam variations and in part from device resolution. (right) Residuals of the scatter plot on the left.

SUMMARY

Beam profile and halo detectors have been developed for transfer lines and external beam lines at Fermilab. The detectors, based on segmented 5μm Ti foils, have been shown to have sufficient beam centroid and width resolutions, and have enabled measurements to be performed at full beam instantaneous intensities with sufficiently low $(\sim3\times10^{-6})$ fractional beam loss.

ACKNOWLEDGMENT

We thank J.D. Gilpatrick of LANL and G. Ferioli of CERN for valuable discussion and advice. We thank the members of the University of Texas at Austin's Physics Department mechanical shops for their efforts toward the chambers' construction, as well as the Fermilab Particle Physics, and Accelerator Divisions for their assistance in integration and installation of the devices. This work was supported by the U.S. Department of Energy and by the Fondren Family Foundation.

REFERENCES

[1] C.Moore et al, Proc. 2003 Part. Accel. Conf., pp1652-1654, Stanford, CA, May, 2003.
[2] See S. Kopp, "The NuMI Beam at Fermilab," Fermilab-Conf-05-093-AD, Proc. 2005 Part. Accel. Conf.
[3] R.Drucker, R.Ford, & G.Tassotto, FERMILAB-Conf-98/062, published Proc. Beam Diag. and Instr. for Part. Acc. (DIPAC), Frascati (Rome), Italy, (1997).
[4] G.Ferioli, private communication.
[5] G.Ferioli and R.Jung, CERN-SL-97-71(BI), published in Proc. Beam Diag. and Instr. for Part. Acc. (DIPAC), Frascati (Rome), Italy, (1997).
[6] Ž.Pavlović et al., Fermilab-TM-2312-AD (2005).
[7] D. Indurthy et al., Fermilab-Conf-04-520, AIP Conf. Proc. 732:341-349 (2004), Proc. 11th Beam Instr. Wkshp (BIW04).
[8] S.Kopp et al, "Beam Test of a Segmented Foil SEM Grid,", Nucl.Instr.Meth.A554(2005)138.
[9] Particle Data Group, http://pdg.lbl.gov.
[10] National Institutes of Standards and Technologies, "Stopping Powers of Electrons, Protons, and Alpha Particles," data available at the URL: http://physics.nist.gov/PhysRefData.
[11] J. Krider and C. Hojvat, Nucl. Instr. Meth. A247, 304 (1986).